X-ray Absorption Spectroscopic Studies of the FeZn Derivative of Uteroferrin[†]

Xuedong Wang, Clayton R. Randall, Anne E. True, and Lawrence Que, Jr.*

Department of Chemistry and Center for Metals in Biocatalysis, University of Minnesota, Minneapolis, Minnesota 55455

Received June 17, 1996; Revised Manuscript Received August 23, 1996[⊗]

ABSTRACT: The FeZn derivative of purple acid phosphatase from porcine uterus (FeZnUf) and its phosphate complex (FeZnUf·PO_4) have been characterized by X-ray absorption spectroscopy at both the iron and zinc K-edges, to gain insight into the nature of the FeZn active site as well as the phosphate binding mode. Pre-edge data show that both FeZnUf and FeZnUf·PO_4 have a 6-coordinate iron site. The iron site has an average Fe−O/N bond length of 2.01−2.02 Å, which can be resolved into subshells of 1.92 and 2.11 Å for FeZnUf·PO_4. On the other hand, the zinc site has a shell of scatterers at 2.02−2.03 Å plus one scatterer at *ca.* 2.4 Å. These metal−ligand bond lengths are consistent with the nature of the ligands deduced from spectroscopic studies or identified in the crystal structure of the related kidney bean purple acid phosphatase (KBPAP). The outer-sphere analysis indicates an Fe−Zn separation of ∼3.3 Å in both FeZnUf and FeZnUf·PO_4, consistent with the presence of an $M_2(\mu\text{-OR})_2$ diamond core as found in the crystal structures of KBPAP, calcineurin, and protein phosphatase 1. The Fe−P and Zn−P bond distances in FeZnUf·PO_4 are determined to be 3.23 and 3.18 Å, respectively, indicating that phosphate binds to the dinuclear center in a bidentate mode; such a mode has been observed in oxoanion complexes of KBPAP, calcineurin, and alkaline phosphatase, as well as in a number of synthetic FeFe and FeZn complexes. The implications of these structural results on the mechanism of phosphatase action are discussed.

Purple acid phosphatases (PAPs) belong to a growing class of metallohydrolases containing bimetallic active sites that catalyze the hydrolysis of phosphate esters. While the physiological function of the PAPs is not well established, the PAP from porcine uterus, uteroferrin (Uf), has been postulated to provide iron for fetal pigs (Doi et al., 1988; Nuttleman et al., 1990), and histochemical studies on bovine spleen PAP (BSPAP) suggest a catabolic role in degrading phosphoproteins of the erythrocyte membrane and cytoskeleton (Schindelmeister et al., 1987). Interestingly, the recently reported crystal structures of kidney bean PAP (KBPAP) (Sträter et al., 1995; Klabunde et al., 1996) and the related protein phosphatase 1 (PP-1) (Egloff et al., 1995; Goldberg et al., 1995) and protein phosphatase 2B (or calcineurin) (Griffith et al., 1995; Kissinger et al., 1995) reveal a striking similarity among the active sites of these three enzymes. In addition, both PAPs and PPs possess phosphoserine/threonine phosphatase activity (Murray et al., 1989), and amino acid sequences of the catalytic regions display surprising homology (Vincent & Averill, 1990). Given the similarity in the structures of the active sites and amino acid sequences, there might be a relationship among the physiological functions of these phosphatases. It is well-known that protein phosphorylation plays a critical role in regulating many cellular processes in eukaryotes, particularly in signal transduction pathways, requiring both a protein kinase and a protein phosphatase. Among the family of protein phosphatases, calcineurin plays an essential role in the T-cell activation pathway; it is a common target of two immunosuppressive drugs, cyclosporin A and FK506 (Liu et al., 1991), for the prevention of graft rejection following organ transplantation and in the treatment of certain autoimmune disorders. PP-1, on the other hand, is the major phosphatase that regulates glycogen metabolism in response to insulin and adrenalin (Dent et al., 1990). Thus, PAPs by analogy may play a similar role in regulating some cellular process.

The active site of KBPAP (Sträter et al., 1995; Klabunde et al., 1996) shown in Figure 1 consists of an iron and a zinc ion bridged by a monodentate aspartate and probably a hydroxide. This $M_2(OR)_2$ diamond core results in an Fe−Zn separation of 3.26 Å. The Fe(III) site is terminally coordinated by tyrosine, histidine, and monodentate aspartate, while the zinc(II) site is terminally coordinated by two histidines and an asparagine. Two solvent molecules complete the coordination spheres of the two metal ions on the same face of the M_2O_2 diamond core. The metal centers in calcineurin and PP-1 have almost identical coordination environments as in KBPAP, except for the absence of the tyrosine ligand. All three active sites are found at the surface of the proteins in a manner suitable for interaction with substrates, suggesting catalytic roles for the metals and a mechanistic connection among them.

Uteroferrin (True et al., 1993) and bovine spleen PAP (Averill et al., 1987) are the best studied mammalian PAPs.

[†] This work is supported by a grant from the National Science Foundation (MCB-9405723 to L.Q.). Beamline X9 at the NSLS at BNL is supported by the National Institutes of Health (RR-001633) and CHESS is supported by the National Science Foundation (DMR-9311772).

[⊗] Abstract published in *Advance ACS Abstracts,* October 15, 1996.

[1] Abbreviations: BSPAP, bovine spleen purple acid phosphatase; ehgs, *N*,*N*′-ethylene(*o*-hydroxyphenylglycine)salicylideneamine; EPR, electron paramagnetic resonance; EXAFS, extended X-ray absorption fine structure; FeZnUf, FeZn derivative of uteroferrin; FeZnUf·PO_4, FeZnUf derivative of uteroferrin complexed with phosphate; Hr, hemerythrin; KBPAP, kidney bean purple acid phosphatase; MMO, methane monooxygenase; MMOH, methane monooxygenase hydroxylase; PAP, purple acid phosphatase; PP, protein phosphatase; PP-1, protein phosphatase 1; salen, *N*,*N*′-ethylenebis(salicylideneamine); Uf, uteroferrin; Uf_r, reduced uteroferrin; XANES, X-ray absorption near-edge structure; XAS, X-ray absorption spectroscopy.

S0006-2960(96)01436-5 CCC: $12.00

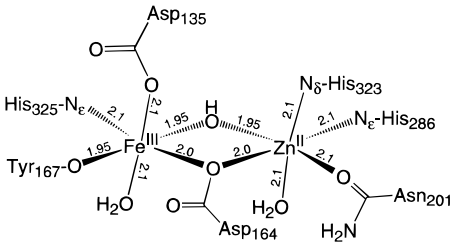

FIGURE 1: Crystal structure of the active site of KBPAP. The metal−ligand bond lengths shown are estimates based on model complexes: Fe(III)−μ−OH (Borer et al., 1983; Bossek et al., 1995; Ou et al., 1978; Thich et al., 1976); Fe(III)−μ−O(carboxylato-O) (Spartalian et al., 1988), Fe(III)−O(Tyr) (Davis et al., 1986; Heistand et al., 1982; Lauffer et al., 1983; Pyrz et al., 1991); Fe(III)−O(carboxylate) (Armstrong & Lippard, 1984; Kitajima et al., 1990; Ménage et al., 1992; Tolman et al., 1991); Fe(III)−N(imidazole) (Gomez-Romero et al., 1988; Tolman et al., 1991; Wu et al., 1990); Fe(III)−O(water) (Dong et al., 1995; Hazell et al., 1994; Murch et al., 1987; Murphy et al., 1982); Zn−μ−OH (Al-Juaid et al., 1986; Bazzicalupi et al., 1995; Chaudhuri et al., 1992; Murthy & Karlin, 1993); Zn−μ−O(carboxylato-O) (Chen et al., 1994; Clegg et al., 1985; Yampolskaya et al., 1987); Zn−O(amide) (Braibanti et al., 1971; Nikolaev et al., 1985; Sabirov et al., 1993); Zn−N(imidazole) (Garrett et al., 1983; Kirchner & Krebs, 1987; Kistenmacher, 1972); Zn−O(water) (Miller et al., 1985; Quiros et al., 1991).

Unlike KBPAP, the mammalian PAPs contain an antiferromagnetically coupled Fe(III)Fe(II) center. However, the Fe(II) site in the mammalian PAPs can be replaced by Zn(II) with no loss of enzymatic activity (Keough et al., 1980; Davis & Averill, 1982). Spectroscopic comparisons of the mammalian PAPs with KBPAP suggest similar active-site structures (Beck et al., 1988; Suerbaum et al., 1993). Indeed, an alignment of the sequences of Uf and KBPAP displays blocks of sequence homology in the metal-coordinating region (Klabunde et al., 1995).

In the absence of a crystal structure, EXAFS becomes an attractive and powerful technique to examine the structure of the metal sites in mammalian PAPs. Previously EXAFS studies on BSPAP (Kauzlarich et al., 1986) and Uf (True et al., 1993) have been reported. The average Fe−O/N ligand bond length is *ca*. 2.0 Å for both enzymes, in agreement with the crystal structure of KBPAP, but these studies only provide a metal coordination environment that is averaged between the Fe(II) and Fe(III) sites. Furthermore, the Fe−Fe distance determined from EXAFS analysis of the active Fe(II)Fe(III) forms ranges from 3.0 to 3.5 Å.

The availability of an enzymatically active FeZnUf provides a unique opportunity to probe the two metal sites independently because of the approximately 2.5-keV difference in the K-absorption edges. Besides information on the coordination environments of the individual metal ions, this approach provides an additional check on structural parameters unique to a dinuclear active site, such as the metal−metal distance and the binding mode of potentially bridging exogenous ligands. In this paper we report the Fe and Zn K-edge EXAFS studies on FeZnUf and FeZnUf·PO_4 and compare our structural conclusions with the published KBPAP structures (Sträter et al., 1995; Klabunde et al., 1996). FeZnUf·PO_4 is of particular interest to provide insight into how the product, phosphate, binds to the dinuclear active site and, by extension, how substrate may interact with the metal sites in the catalytic mechanism.

EXPERIMENTAL PROCEDURES

Preparation of Samples. Uteroferrin was isolated and purified from the uteri of gilts treated with β-estradiol 17-valerate according to the literature procedures (Basha et al., 1980; Pyrz et al., 1986). FeZnUf was then prepared (Keough et al., 1980) and exhibited a specific activity of about 350 units/mg, comparable to that of native uteroferrin. It featured a visible spectrum with λ_{max} at 530 nm ($\epsilon = 4000$ M^{-1} cm^{-1}) (David & Que, 1990), and metal analyses gave values of 1.0 ± 0.1 Fe and 1.0 ± 0.1 Zn atoms/molecule of FeZnUf. The amount of diiron Uf in the FeZnUf sample was less than 5% as determined by quantitation of its characteristic EPR signal. FeZnUf·PO_4 was prepared by adding a saturating amount of phosphate to the concentrated FeZnUf solution in acetate buffer at pH 4.9; the final concentrations of protein and phosphate were 4.5 and 50 mM, respectively. The EPR spectrum of the FeZnUf·PO_4 sample verified the absence of free FeZnUf. The XAS samples were diluted with glycerol (20% by volume) to prevent ice crystal formation when the samples were frozen and placed in gold-plated copper sample holders.

X-ray Absorption Spectroscopy. X-ray absorption data of both the iron and zinc K-edges of FeZnUf and FeZnUf·PO_4 were collected at beamline X9 of the National Synchrotron Light Source (NSLS) at Brookhaven National Laboratory and stations C2 and A3 of the Cornell High Energy Synchrotron Source (CHESS). The X-ray absorption spectra at the iron K-edge were collected between 6.95 and 8.0 keV and the monochromator was calibrated using the 7113.0-eV 1s → 3d pre-edge peak of the XAS spectrum of [Et_4N][$FeCl_4$]. The Zn K-edge spectra were collected between 9.46 and 10.35 keV, and the monochromator was calibrated using the edge energy of zinc foil at 9662.0 eV. The XAS data were obtained in fluorescence mode from the protein samples frozen at 77 K. The A_{exp} (C_f/C_0) was determined from an incident (C_0) ionization detector and a final fluorescence (C_f) detector, the latter being either a large solid-angle Lytle detector with a Mn filter (for iron K-edge measurements) or a Cu filter (for zinc K-edge measurements) or a Canberra 13-element Ge solid state detector.

The treatment of raw EXAFS data to yield χ has been discussed in detail in review articles (Scott, 1985; Teo, 1981). A modification of the EXAPLT program was employed to extract χ from A_{exp} by using a cubic spline function, including preliminary baseline correction and correction of fluorescence data for thickness effects and detector response (Scarrow et al., 1987). The refinements reported were on $k^3\chi$ data and the function minimized was $R = \{\Sigma\, k^6(\chi_c - \chi)^2/N\}^{1/2}$, where the sum is over N data points between 2 and 14 $Å^{-1}$.

Single-scattering EXAFS theory allows the total EXAFS spectrum to be described as the sum of shells of separately modeled atoms using the following equation (Scarrow et al., 1987):

$$\chi_c = \Sigma\, nA[f(k)k^{-1}r^{-2}\exp(-2\sigma^2k^2)\sin(2kr + \alpha(k))]$$

where n is the number of atoms in the shell, $k = [8\pi^2m_e(E - E_0 + \Delta E)/h^2]^{1/2}$, and σ^2 is the Debye−Waller factor. Phase [$\alpha(k)$] and amplitude [$f(k)$] functions were theoretically calculated using a curved-wave formalism (McKale et al., 1988). A variation of FABM (fine adjustment based on models) was then used in the analysis procedure to obtain

the amplitude reduction factor (A) and the shell-specific edge shift (ΔE), which are empirical parameters that partially compensate for imperfections in the theoretical amplitude and phase functions (Teo et al., 1983). A and ΔE values were determined by using a series of crystallographically characterized model complexes. For each shell, two parameters were refined at one time (r and n or σ^2). The fitting results provide the average metal−ligand distances, the type and the number of scatterers, and the Debye−Waller factors, which can be used to evaluate the distribution of Fe− or Zn−ligand bond lengths in each shell. The EXAFS goodness of fit criterion applied here is

$$\epsilon^2 = [(N_{idp}/\nu)\cdot\Sigma\,(\chi_c - \chi)^2/\sigma^2]/N$$

as recommended by the International Committee on Standards and Criteria in EXAFS (Bunker et al., 1991; Riggs-Gelasco et al., 1995), where ν is the number of degrees of freedom calculated as $\nu = N_{idp} - N_{var}$, N_{idp} is the number of independent data points, and N_{var} is the number of variables that are refined. N_{idp} is calculated as $N_{idp} = 2\Delta k\Delta R/\pi + 2$ (Stern, 1993). The use of ϵ^2 as criterion for the goodness of fit allows us to compare fits using different numbers of variable parameters.

The pre-edge areas were calculated by subtracting an arctangent function from the data and normalizing with respect to the edge jump height. The background function was determined by a least-squares fit of an arctangent together with a first-order polynomial to the data below the inflection point to the edge (Roe et al., 1984; Randall et al.; 1995). The edge jump was determined by fitting a first-order polynomial to the data. The pre-edge area after the background subtraction was obtained by integrating over a range of about 8 eV. This range centered on the peak and any residual background function was interpolated over that range. The difference between the two lines at the inflection point was used as normalization factor for the pre-edge area. The normalized pre-edge area is reported as percent of edge height × eV. For example, Na[Fe(EDTA)(H_2O)] has a normalized pre-edge area of 0.081 eV, which is abbreviated as 8.1 units.

RESULTS

Pre-Edge Data. The X-ray absorption spectra of iron complexes contain a small peak at about 10 eV below the midpoint of the K-absorption edge, which is assigned to the 1s → 3d transition. XANES studies and molecular orbital calculations on iron(III) model compounds have demonstrated that the intensity of the pre-edge feature relative to the edge jump can be correlated with the amount of iron 4p and 3d orbital mixing and, consequently, with the metal coordination geometry (Roe et al., 1984). In general, the pre-edge peak intensity increases as the metal coordination environment deviates from inversion symmetry and therefore $I_{tetrahedral} > I_{5-coord} > I_{octahedral}$. From the pre-edge database for Fe(III) complexes, 4-coordinate complexes have pre-edge peak areas ranging from 23 to 25 units, 5-coordinate complexes from 12 to 19 units, and 6- or 7-coordinate complexes from 6 to 9 units (Roe et al., 1984).

The positions of the Fe K-edge of FeZnUf and FeZnUf·PO_4 (7124.0 and 7123.2 eV) are consistent with the iron being in the +3 oxidation state. The 1s → 3d pre-edge areas for FeZnUf and FeZnUf·PO_4 are 7.2 and 7.6 units, respectively, as shown in Figure 2. These values are consistent with those found for 6-coordinate mononuclear iron(III) complexes or weakly coupled diiron(III) complexes. It is also very close to the values of Uf_o·PO_4 and Uf_o·AsO_4 (6.8 and 7.4 units, respectively) (True et al., 1993), which are proposed to have 6-coordinate Fe(III) sites. Thus, the Fe(III) sites of both FeZnUf and FeZnUf·PO_4 are proposed to be 6-coordinate.

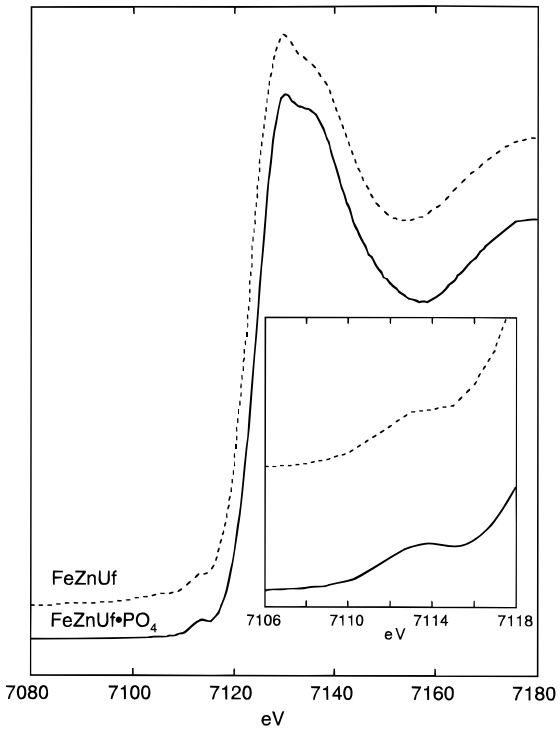

FIGURE 2: Fe K-edge XANES spectra of FeZnUf and FeZnUf ·PO_4. The inset is a magnification of the 1s → 3d pre-edge transition.

First-Sphere EXAFS Analysis. The raw $k^3\chi$ EXAFS data for both FeZnUf and FeZnUf·PO_4 are presented in Figure 3. The zinc K-edge spectra are less noisy than the iron K-edge spectra because the higher energy X-rays at the zinc K-edge can penetrate the sample more effectively and give rise to more intense fluorescence. The Fe K-edge data for FeZnUf·PO_4 appear superior to those of FeZnUf due to the greater homogeneity of the iron center in FeZnUf·PO_4, as earlier indicated by the sharpness of its EPR spectrum (David & Que, 1990).

The first-sphere simulation results for the iron K-edge data are summarized in Table 1. An average first-shell coordination of 5 or 6 O/N at 2.01−2.02 Å for both FeZnUf and FeZnUf·PO_4 was found, suggesting that the first-shell coordination at the iron site in FeZnUf does not change significantly upon the addition of phosphate. Since coordination numbers from EXAFS fits typically have an uncertainty of 20% (Cramer, 1988), the EXAFS fits are consistent with the pre-edge analysis. The Debye−Waller factors obtained for the single-shell fits are fairly large, indicating a broad range of distances being represented by this shell. The more limited resolution of the FeZnUf data did not allow the splitting of this shell, while the first sphere of FeZnUf·PO_4 could be fit with two shells of scatterers at *ca*. 1.9 and 2.1 Å. The two-shell fits afforded ϵ^2 values considerably smaller than the one-shell fits.

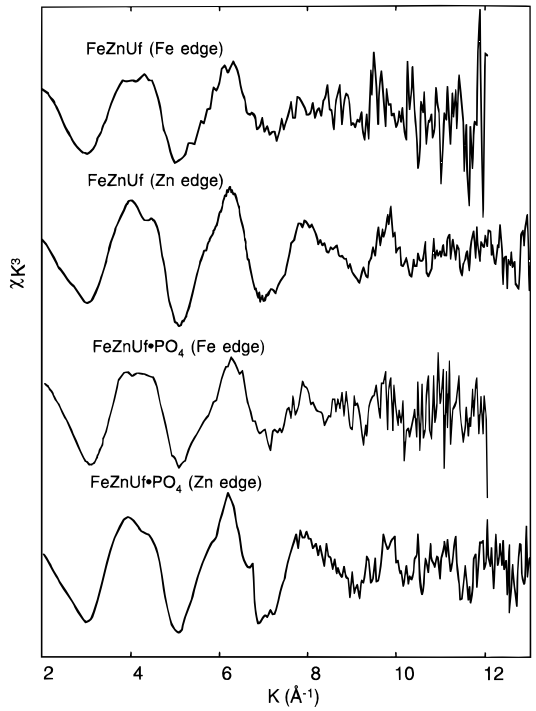

FIGURE 3: Raw EXAFS data ($k^3\chi$) obtained for Fe and Zn K-edge of FeZnUf and FeZnUf·PO_4.

Table 1: First-Sphere EXAFS Fits to the Fourier-Filtered Data (Fe K-Edge)[a]

	Fe−O/N			Fe−O/N			
fit	*n*	*r*	σ^2	*n*	*r*	σ^2	ϵ^2 (10^4)
			FeZnUf				
A	6	2.02	0.017				4.2
B	5	2.02	0.013				1.1
			FeZnUf·PO_4				
C	6	2.01	0.015				6.7
D	5	2.01	0.012				6.7
E	4	2.10	0.004	2	1.91	0.004	3.4
F	3	2.12	0.003	3	1.94	0.007	3.0
G	3	2.12	0.003	2	1.94	0.002	1.2

[a] Fourier transform range = 2−11 $Å^{-1}$ for FeZnUf and 2−12 $Å^{-1}$ for FeZnUf·PO4. Backtransform range = 1.0−2.0 Å for FeZnUf and 1.0−2.3 Å for FeZnUf·PO_4.

Similar to the iron K-edge data, the zinc K-edge data of both FeZnUf and FeZnUf·PO_4 could be simulated with a single shell of scatterers at 2.02−2.03 Å with fairly large ϵ^2 values (Table 2). Though no improvements to the fits were obtained by splitting the first sphere into two shells of scatterers, the inclusion of a low-Z scatterer at *ca.* 2.4 Å made a notable improvement in ϵ^2 to the fits of both FeZnUf and FeZnUf·PO_4. A distinct perturbation of the oscillations at $k \sim 11$ $Å^{-1}$ was observed in the first-sphere Fourier-filtered spectrum of FeZnUf·PO_4 (Figure 4), and it could only be duplicated with the presence of three shells (fit I, Table 2).

Outer-Sphere EXAFS Analysis. The Fe−Zn separation and the presence of phosphate in the coordination sphere of the dinuclear site can be determined from the analysis of the outer-sphere EXAFS data. The first-sphere parameters used to achieve the outer-sphere fits were chosen from fits B and G in Table 1 for the iron K-edge of FeZnUf and FeZnUf·PO_4, respectively, and fits D and I in Table 2 for the zinc K-edge data of FeZnUf and FeZnUf·PO_4, respectively.

Table 2: First-Sphere EXAFS Fits to the Fourier-Filtered Data (Zn K-Edge)[a]

	Zn−O/N			Zn−O/N			Zn−O/C			
fit	*n*	*r*	σ^2	*n*	*r*	σ^2	*n*	*r*	σ^2	ϵ^2 (10^4)
					FeZnUf					
A	5	2.02	0.009							6.5
B	4	2.02	0.006							3.8
C	5	2.02	0.009				1	2.42	0.002	3.7
D	4	2.02	0.006				1	2.44	0.002	2.3
					FeZnUf·PO_4					
E	5	2.03	0.009							7.4
F	4	2.02	0.007							6.6
G	3	2.09	0.003	2	1.95	0.002				8.7
H	5	2.03	0.009				1	2.46	0.002	3.2
I	3	2.10	0.004	2	1.96	0.002	1	2.45	0.003	1.5

[a] Fourier transform range = 2−13 $Å^{-1}$ for FeZnUf and FeZnUf·PO_4. Backtransform range = 1.0−2.3 Å for FeZnUf and 1.1−2.3 Å for FeZnUf·PO_4.

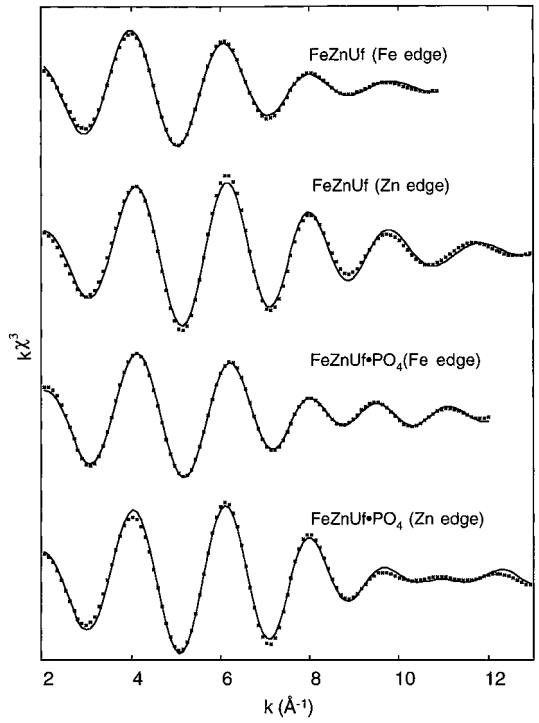

FIGURE 4: Fourier-filtered $k^3\chi$ EXAFS data (■) and first-sphere fits (—) of Fe K-edges of FeZnUf and FeZnUf·PO_4 (fits B and G in Table 1) and Zn K-edges of FeZnUf and FeZnUf·PO_4 (fits D and I in Table 2).

The Fourier transforms of the filtered $k^3\chi$ iron and zinc K-edge EXAFS data of FeZnUf in Figure 5 show several weak second-shell features. Since there is strong spectroscopic evidence that uteroferrin contains a dinuclear active site (Antanaitis et al., 1983), one of these features must correspond to a metal scatterer. The weak outer-shell scattering can arise from destructive interference of M−M′ and M−C scattering at similar distances as noted in the Cu EXAFS of a series of CuFe dinuclear complexes (Scott & Eidsness, 1988). In the fits to the Fe K-edge data, a Zn scatterer at either 3.0 or 3.4 Å decreased the ϵ^2 value, with the latter affording the smaller ϵ^2 and σ^2 values (Table 3). Similarly in the fits to the Zn K-edge data, an Fe scatterer at 3.0 or 3.3 Å decreased the ϵ^2 value, with the latter also giving rise to the smaller ϵ^2 and σ^2 values. The fits to both

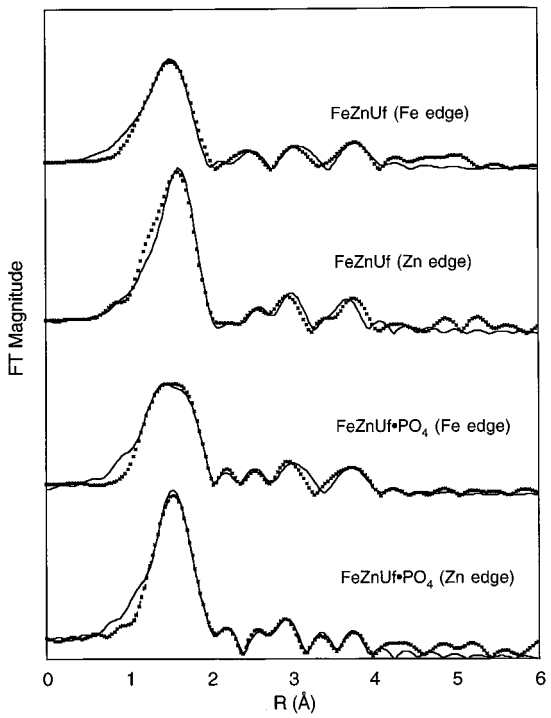

FIGURE 5: Fourier-transform of EXAFS data (■) and outer-sphere fits (—) of Fe, Zn K-edges of FeZnUf (fits E and K in Table 3) and Fe, Zn K-edges of FeZnUf•PO_4 (fits E and K in Table 4).

Table 3: Outer-Sphere Fits to the Fourier-Filtered $k^3\chi$ Data of FeZnUf

	M−M′			M−C			M−C				
fit	*n*	*r*	σ^2	*n*	*r*	σ^2	*n*	*r*	σ^2	$\epsilon^2(10^4)^a$	$\epsilon^2(10^4)^b$
					Fe K-Edge						
A	1	3.00	0.016							7.2	
B	1	3.38	0.011							5.4	
C	1	3.01	0.012	2	3.32	0.006				4.3	
D	1	3.37	0.009	2	3.15	0.007				2.8	8.6
E	1	3.37	0.009	2	3.15	0.007	2	4.08	0.003		5.0
F	1	4.04	0.007	2	3.20	0.24					7.9
					Zn K-Edge						
G	1	2.96	0.012							6.1	
H	1	3.29	0.009							5.6	
I	1	2.99	0.011	4	3.36	0.003				4.8	
J	1	3.27	0.006	4	3.14	0.008				3.6	7.6
K	1	3.27	0.006	4	3.14	0.008	4	4.05	0.005		4.6
L	1	3.90	0.014	4	3.26	0.039					9.9

[a] Backtransform range = 1−3.35 Å for Fe K-edge and 1−3.3 Å for Zn K-edge, and ϵ^2 values for fit B in Table 1 and fit F in Table 2 are 7.2×10^{-4} and 6.2×10^{-4}, respectively. [b] Backtransform range = 1.0−4.1 Å for Fe K-edge and 1.0-4.0 Å for Zn K-edge.

the Fe and Zn K-edge data were improved by the addition of a C shell, which presumably derives from the second-shell carbon atoms of the histidine ligands. As in the metal-only fits, the smaller ϵ^2 and σ^2 values were associated with fits having a metal scatterer at 3.3−3.4 Å and carbon scatterers at ∼3.1 Å. Indeed the alternative assignment would require C scatterers at 3.3 Å, which is a distance somewhat longer than would be reasonable for the second-shell carbon atoms of histidine ligands. A number of C scatterers at *ca.* 4.1 Å are further required to simulate the features around 3.8 Å in the Fourier transform spectra of both Fe and Zn K-edge data (fits E and K, Table 3), which are associated with the outer-shell C and N atoms of coordinated histidines.

Table 4: Outer-Sphere Fits to the Fourier-Filtered $k^3\chi$ Data of FeZnUf•PO_4

	M−M′			M−P			M−C				
fit	*n*	*r*	σ^2	*n*	*r*	σ^2	*n*	*r*	σ^2	$\epsilon^2(10^4)^a$	$\epsilon^2(10^4)^b$
					Fe K-Edge						
A	1	2.96	0.013							7.6	
B	1	3.34	0.008							2.2	
C	1	2.99	0.014	1	3.49	0.004				2.2	
D	1	3.33	0.007	1	3.23	0.014				0.9	8.2
E	1	3.33	0.007	1	3.23	0.014	2	4.01	0.001		5.9
F	1	3.71	0.008	1	3.14	0.008				7.6	
					Zn K-Edge						
G	1	2.95	0.013							7.7	
H	1	3.29	0.008							4.8	
I	1	2.96	0.012	1	3.43	0.003				2.4	
J	1	3.26	0.004	1	3.19	0.004				2.4	7.0
K	1	3.25	0.005	1	3.18	0.003	4	4.07	0.004		3.6
L	1	3.65	0.003	1	3.11	0.006				8.2	

[a] Backtransform range = 1.0−3.3 Å for Fe K-edge and 1.1−3.1 Å for Zn K-edge, and ϵ^2 values for fit G in Table 1 and fit K in Table 2 are 9.0×10^{-4} and 7.0×10^{-4}, respectively. [b] Backtransform range = 1.0−4.0 Å for Fe K-edge and 1.1-4.0 Å for Zn K-edge.

For FeZnUf•PO_4, the outer-sphere simulation results are shown in Table 4. In the fits to the iron K-edge data, the inclusion of a Zn scatterer at ∼3.3 Å significantly decreased the ϵ^2 value, while a Zn scatterer at ∼3.0 Å hardly affected the ϵ^2 value. Since previous EPR studies of FeZnUf complexed with ^{17}O-labeled phosphate clearly demonstrated that phosphate was coordinated to the Fe(III) site, a phosphorus shell was also introduced into the fits. Indeed, the presence of phosphorus at the Fe(III) site of FeZnUf•PO_4 improved the fits dramatically by decreasing the ϵ^2 values 2−3-fold. Fit D with a Zn scatterer at 3.33 Å and a P scatterer at 3.23 Å (fit D, Table 4) was favored because of its smaller ϵ^2 value and the smaller σ^2 values for the Zn shell. However, the Debye−Waller factor for the P shell was fairly large which indicates a large, disorder (either static or dynamic) between the Fe and P atoms.

For the Zn K-edge data of FeZnUf•PO_4, a good fit was obtained with a Zn−Fe distance of 3.26 Å and a Zn−P distance of 3.19 Å (fit J, Table 4). Similar to the Fe K-edge fits, the inclusion of the phosphorus shell in the Zn fits decreased the ϵ^2 value by 2-fold. Unlike the Fe K-edge result, the Debye−Waller factor of the P shell in the best fit of the Zn K-edge data was small. The alternative fit with a Zn−Fe distance of 2.96 Å and a Zn−P distance of 3.43 Å produced a reasonably low ϵ^2 value as well, but the Debye−Waller factor of the Fe shell was quite large. The difference between the results for FeZnUf•PO_4 and FeZnUf is the scatterer at *ca.* 3.2 Å, which is attributed to P for FeZnUf•PO_4 and C for FeZnUf. When a C shell at *ca.* 3.2 Å was introduced in place of the P scatterer in the fits of the Fe and Zn K-edge data of FeZnUf•PO_4, negative σ^2 values for the C shell were required to fit the data, a result which is unacceptable (data not shown). Similar to FeZnUf, the fits for FeZnUf•PO_4 require the inclusion of a C shell at *ca.* 4.1 Å to reproduce the peaks at 3.8 Å in the Fourier transform spectra (fits E and K, Table 4), which correspond to the outer-shell features of the coordinated His residues.

Combining the results from the Fe and the Zn K-edge data, we conclude that FeZnUf and FeZnUf•PO_4 have an Fe−Zn distance of ∼3.3 Å, while the latter has Fe− and Zn−P distances of ∼3.2 Å. Our results contrast with those in a

previous EXAFS report, which found an Fe−Zn distance of 3.9 Å for KBPAP and 3.7 Å for the KBPAP−phosphate complex (Priggemeyer et al., 1995). Fits with an Fe−Zn distance of *ca.* 3.9 Å and 3.7 Å for FeZnUf and FeZnUf·PO_4, respectively, could be obtained, but these fits reproduced the Fourier-transformed spectral features poorly and were associated with larger ϵ^2 or unreasonable σ^2 values (fits F and L, Table 3; fits F and L, Table 4).

DISCUSSION

The X-ray absorption spectroscopic analysis reported here indicates that both the iron and zinc sites of FeZnUf and FeZnUf·PO_4 are coordinated only by low-Z (O/N) ligands. The pre-edge data indicate 6-coordinate structures for the iron sites of both FeZnUf and FeZnUf·PO_4. These conclusions agree with the crystal structure of KBPAP which shows a novel Fe(III)−Zn(II) active site wherein the metal ions are bridged by a hydroxide and a monodentate aspartate and coordinated by terminal Tyr, Asp, His, and solvent ligands on the Fe(III) ion and terminal Asn, His and solvent ligands on the Zn(II) ion (Figure 1) (Sträter et al., 1995; Klabunde et al., 1996). Similar bimetallic sites are found for the related calcineurin and protein phosphatase 1 except for the replacement of the tyrosine and histidine on the Fe(III) site by histidine and water, respectively (Egloff et al., 1995; Goldberg et al., 1995; Griffith et al., 1995; Kissinger et al., 1995). Since there is sequence homology between KBPAP and uteroferrin in the region of the metal-coordinating residues (Klabunde et al., 1995), a very similar coordination environment for the bimetallic center of uteroferrin is likely.

Figure 1 also includes the estimated bond lengths of the metal ligands in the coordination sphere of PAPs based on crystallographically characterized model complexes. The first-sphere fits to the EXAFS data of FeZnUf and FeZnUf·PO_4 are in good agreement with these estimated values. The average Fe−ligand distance of the Fe site of FeZnUf is 2.02 Å, while that of FeZnUf·PO_4 is 2.01 Å. Because of the better quality and higher *k* range of the FeZnUf·PO_4 data, the first coordination sphere of the Fe site can be resolved into two shells, consisting of 2 O/N scatterers at 1.92 Å and 3−4 O/N scatterers at 2.11 Å. Similarly, the Zn site of FeZnUf·PO_4 is best fit with three shells, 2 scatterers at 1.96 Å, 3 scatterers at 2.10 Å, and 1 scatterer at 2.45 Å. The average distance of the shorter two shells, 2.03 Å, also agrees well with the 2.02-Å shell from the fit of the FeZnUf data.

The 1.92-Å shell on the Fe site of FeZnUf·PO_4 most likely corresponds to the terminal tyrosinate (1.9 Å) and the bridging hydroxide (1.95 Å). Phenolates typically give rise to Fe(III)−O bonds of 1.85−1.92 Å (Davis et al., 1986; Heistand et al., 1982; Lauffer et al., 1983; Pyrz et al., 1991), while hydroxo bridges afford Fe(III)−O bonds of 1.95−2.00 Å (Armstrong & Lippard, 1984; Bossek et al., 1995; Thich et al., 1976; Turowski et al., 1994). The 2.1-Å shell would then be associated with the two Asp residues, the His, and the phosphate oxygen.

On the other hand, the 1.96-Å shell on the Zn site is assigned to the bridging hydroxide and aspartate, these being the only anionic ligands bound to the Zn center. The Zn(II)−O bond in a hydroxo-bridged dizinc complex averages 1.96 Å (Al-Juaid et al., 1986; Bazzicalupi et al., 1995; Chaudhuri et al., 1992; Murthy & Karlin, 1993), while the Zn(II)−O bond of a monodentate carboxylate bridge in a dizinc(II) complex can be as short as 1.95 Å (Clegg et al., 1985; Yampolskaya et al., 1987). The 2.1-Å shell may then be associated with the His residues, the Asn carbonyl, and the phosphate.

One unexpected result from the fits is the requirement for a scatterer at *ca.* 2.4 Å on the Zn site. Such a scatterer was also required in fits to data on uteroferrin with the native diiron site, though it was not possible to specify which metal site was involved (True et al., 1993). In other EXAFS papers, we have associated a 2.4-Å scatterer with the carbon atom of a chelated carboxylate (Kitajima et al., 1994; True et al., 1990, 1993); however, it is clear from the phosphatase crystal structures that neither carboxylate ligand associated with the dinuclear center is chelated (Egloff et al., 1995; Goldberg et al., 1995; Griffith et al., 1995; Kissinger et al., 1995; Sträter et al., 1995; Klabunde et al., 1996). In addition, the carbonyl oxygen of the bridging aspartate is oriented away from the metal centers.

Among the Zn ligands, two candidates for the 2.4-Å scatterer are the Asn and the N_ϵ-bound His. An amide carbonyl is usually considered a weak ligand and only recently has such a residue been shown to ligate a transition metal in metalloproteins, *e.g.*, lipoxygenase (Minor et al., 1993), isopenicillin N synthase (Roach et al., 1995), and the protein phosphatases (Egloff et al., 1995; Goldberg et al., 1995; Griffith et al., 1995; Kissinger et al., 1995; Sträter et al., 1995; Klabunde et al., 1996). Several crystal structures of zinc−amide complexes are available, and a Zn−O bond length of 2.1 Å is typically observed (Braibanti et al., 1971; Nikolaev et al., 1985; Sabirov et al., 1993). However, the other ligands in these model complexes are fairly weak, with metal−ligand distances of 2.1−2.2 Å. It could be argued that the more strongly bound ligands like the bridging hydroxide and aspartate in FeZnUf and FeZnUf·PO_4 would neutralize the Lewis acidity of the Zn ion, resulting in longer bonds for the neutral ligands. The ligand at the position trans to the hydroxide bridge may be particularly affected, which in the case of KBPAP is the Asn ligand (Sträter et al., 1995; Klabunde et al., 1996).

Alternatively, one of the Zn−N(His) bonds could also be lengthened by constraints in the active site. In fact, only two of the three His ligands found in the crystal structure of KBPAP have been identified from the NMR studies of the PAPs from porcine uterus and bovine spleen (Scarrow et al., 1990; Wang et al., 1992), the N_ϵ-bound His of the Fe(III) site and the N_δ-bound His of the M(II) site; the third His, which is N_ϵ-bound to the M(II) site, was not observed. If this ligand were coordinated at 2.4 Å, instead of the more typical 2.1 Å, the paramagnetic shift experienced by the N−H proton would be significantly attenuated and not observed outside the diamagnetic region (0−15 ppm).

The average Fe−ligand bond length hardly changes from FeZnUf to FeZnUf·PO_4 from EXAFS analysis (Table 1). Thus the *ca.* 2.1-Å metal−phosphate bonds in FeZnUf·PO_4 must be replaced by metal−solvent bonds of similar length in FeZnUf. The presence of a water ligand at the Zn center would be consistent with the 2.1-Å bond length; it is also unlikely that a Zn−OH moiety would exist at pH 5, pK_as of Zn(II)-bound water ligands being 7 or greater (Kimura, 1994). The 2.1-Å bond length on the Fe(III) center would also be more consistent with a water ligand, since Fe(III)−OH bonds are typically 1.9 Å in length (Dong et al.,1995; Hazell et al., 1994). At best, there may be an equilibrium

between a bound water and hydroxide as suggested by the pK_a of *ca.* 5 associated with the pH dependences of spectroscopic, rapid kinetic, and steady-state kinetic properties (Aquino et al., 1994; Dietrich et al., 1991; Pyrz et al., 1986).

Our EXAFS analysis of both the iron and zinc K-edge data reveals that the iron−zinc distances of FeZnUf and FeZnUf·PO_4 are ∼3.3 Å, in excellent agreement with the metal−metal separation (3.26 Å) found in the KBPAP crystal structure (Sträter et al., 1995; Klabunde et al., 1996) and those of other phosphatases with a (μ-hydroxo)(μ-O-aspartato)dimetal core (Egloff et al., 1995; Goldberg et al., 1995; Griffith et al., 1995; Kissinger et al., 1995). The alternative fits with the Fe−Zn distances of 3.0 Å for both FeZnUf and FeZnUf·PO_4 have been rejected because of the larger σ^2 values associated with the Fe and Zn scatterers (fits C and I in Table 3; fits C and I in Table 4). The presence of two single-atom bridges in the $M_2(OR)_2$ diamond core of FeZnUf and FeZnUf·PO_4 would be expected to afford small Debye−Waller factors for the Fe or Zn shell in the EXAFS analysis because of the rigidity of such a core structure. The 3.3-Å distance is slightly longer than typically found for diiron(III) (Borer et al., 1983; Chiari et al., 1984; Ménage & Que, 1990; Taft & Lippard, 1990; Walker & Poli, 1990) and dizinc(II) (Chaudhuri et al., 1992; Kimura et al., 1994; Murthy & Karlin, 1993) complexes with bis(μ-hydroxo or alkoxo) cores (3.0−3.2 Å) but is comparable to that of the closest synthetic analogue with a monodentate carboxylate bridge. This analogue is a diiron(III) complex, [$Fe^{III}_2(OCH_3)$-(salen)(ehgs)], which has a (μ-methoxo)(μ-O-carboxylato)-diiron(III) core with an Fe−Fe distance of 3.24 Å (Spartalian et al., 1988). This distance may be expected to increase when Zn(II) replaces an Fe(III) because of the increase in ionic radius from Fe(III) (high-spin 6-coordinate, 0.785 Å) to Zn(II) (6-coordinate, 0.885 Å).

The metal−metal distance in FeZnUf is shorter than those in semimetHr azide (3.46 Å) (Scarrow et al., 1987) and mixed-valence MMO hydroxylase (3.42 Å) (DeWitt et al., 1991), whose distances indicate a (μ-hydroxo)diiron(II,III) unit supported by bidentate carboxylate bridges (Bossek et al., 1995). In our earlier EXAFS analysis of the diiron Uf_r, we favored the fit with an Fe−Fe separation of 3.5 Å, and a core structure similar to semimetHr azide and mixed-valence MMOH was proposed (True et al., 1993). However, the alternative fit with an Fe−Fe distance of 3.15 Å which is consistent with the presence of an Fe_2O_2 diamond core could not be ruled out; indeed, a diamond core structure was deduced for the diiron(III) form of uteroferrin based on the 3.3-Å Fe−Fe separation obtained from the fits. A recent EXAFS study on KBPAP deduced an Fe−Zn separation of 3.9 Å, a value which is clearly much longer than that obtained from the crystal structure (Priggemeyer et al., 1995). Our attempts to fit the FeZnUf data with a much longer FeZn distance resulted in significantly poorer fits (fits F and L, Table 4). Given the Fe−Zn separations obtained from EXAFS for FeZnUf and from crystallography for KBPAP, it would seem likely that native uteroferrin and FeZnUf have very similar active-site structures, and this notion would be consistent with the fact that all the enzyme activity is conserved when Fe(II) is substituted by Zn(II) (David & Que, 1990; Keough et al., 1980).

Our EXAFS analysis of FeZnUf·PO_4 clearly demonstrates the presence of a P scatterer *ca.* 3.2 Å away from both the

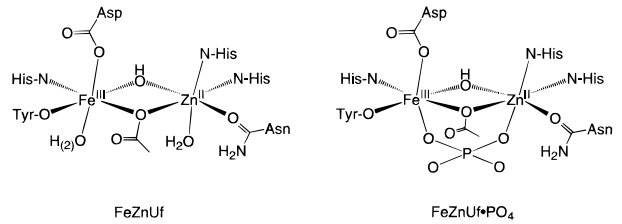

FIGURE 6: Proposed structure for the dinuclear sites of FeZnUf and FeZnUf·PO_4.

Fe and Zn centers, suggesting that phosphate bridges the Fe−Zn unit, as found for the dimetal sites of KBPAP (Klabunde et al., 1996), calcineurin (Griffith et al., 1995), and alkaline phosphatase (Kim & Wyckoff, 1991). The bidentate bridging coordination mode is further precedented by a number of FeFe and FeZn complexes, which show M−P distances of *ca.* 3.2 Å (Drüeke et al., 1989; Jang et al., 1993; Schepers et al., 1990; Turowski et al., 1994; Krebs et al., 1994). Such a bidentate bridging mode for phosphate is also consistent with the Mössbauer data of Uf_r·PO_4, showing that the ΔE_Q values of both the Fe(II) and Fe(III) site are affected by phosphate binding to Uf_r (Pyrz et al., 1986). Interestingly, the Debye−Waller factor of the phosphorus shell at the Fe(III) site is somewhat larger than that of the Zn(II) site, suggesting a larger disorder in the Fe−P distance. Perhaps this observation indicates that the Fe(III) center, with already four anionic ligands, has a weaker affinity for the phosphate than the Zn(II) center. Alternatively, there may be two forms of the phosphate complex, such as a monodentate phosphate coordinated at the Zn(II) site in equilibrium with a bidentate bridging phosphate. However, the very sharp EPR spectrum of FeZnUf·PO_4 (David & Que, 1990) argues against this possibility.

Figure 6 shows the proposed structures for FeZnUf and FeZnUf·PO_4 on the basis of the structural information obtained from our EXAFS analysis and previous spectroscopic studies. Uteroferrin thus resembles KBPAP, calcineurin, and PP-1 in having an M_2O_2 diamond core upon which phosphate ester hydrolysis occurs. This subset of metallohydrolases can further be divided into two subclasses. Uteroferrin and KBPAP have one iron(III) and one divalent ion in the core, and a tyrosine ligand is present in this site in order to stabilize the iron(III); these enzymes have pH optima near pH 5. The other two, on the other hand, do not have a tyrosine ligand and exhibit maximal activity near physiological pH.

Our EXAFS analysis of FeZnUf·PO_4 indicates that phosphate and, by extension, substrate coordinate to the bimetallic site in PAP. An S_N2-type mechanism has been proposed for the PAPs, as indicated by the inversion of configuration at phosphorus upon hydrolysis of a chiral phosphate ester (Mueller et al., 1993). The hydroxide nucleophile required by such a mechanism would thus have to be generated by the bimetallic active site. This is a likely role for the iron(III) ion, because of its high Lewis acidity, particularly considering the acidic pH optimum of the enzyme. Rapid kinetic studies on the binding of phosphate to uteroferrin show that the iron(III) site is not the initial binding site for phosphate (Aquino et al., 1994). Indeed, substrate has been proposed to bind initially at the divalent metal site followed by nucleophilic attack of a hydroxide bound to the Fe(III) site (Aquino et al., 1994; Dietrich et al., 1991; Sträter et al., 1995; Klabunde et al., 1996). The

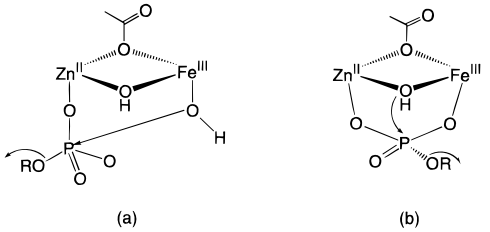

FIGURE 7: Proposed mechanistic schemes involving (a) a terminal hydroxide or (b) a bridging hydroxide for phosphate hydrolysis catalyzed by PAPs.

nucleophile may be the hydroxide terminally coordinated to the Fe(III) site as shown in Figure 7a or the bridging hydroxide as shown in Figure 7b.

The terminal hydroxide model is favored by a number of workers (Aquino et al., 1994; Dietrich et al., 1991; Sträter et al., 1995; Klabunde et al., 1996). In support of this model, the pK_a value determined to be 4−5 from the pH dependences of specific activity, phosphate binding, and the EPR and visible spectra is associated with the ionization of the terminally bound solvent ligand on the Fe(III) center (Pyrz et al., 1986; Aquino et al., 1994; Dietrich et al., 1991). Thus, at the optimum pH (4.9), the solvent-derived ligand on the Fe(III) site appears as hydroxide in Figure 7a to act as the nucleophile in the catalysis, although the EXAFS analysis for FeZnUf is ambiguous on this point. Since most of those experiments were performed in the presence of phosphate or substrate, the ionization of the solvent ligand to form the nucleophile that attacks the phosphate ester may occur only when substrate is bound.

The alternative nucleophile is the hydroxide bridge (Figure 7b). Such a mechanism has been proposed for human PP-1 and bovine calcineurin on the basis of their crystal structures, in which the hydroxo bridge and the substrate (as modeled by a tetraoxo anion) are arranged in a geometry that is favorable for nucleophilic attack on the phosphorus (Egloff et al., 1995; Griffith et al., 1995). Precedents for a bridging hydroxide acting as the nucleophile can be found in the hydrolysis of phosphate esters by a (μ-hydroxo)dizinc(II) and a (μ-hydroxo)dicobalt(III) complex (Chapman & Breslow, 1995; Wahnon et al., 1995). In such a mechanism, the phosphate ester substrate would presumably displace the solvent molecules on the face of the diamond core and bridge the bimetallic active site and thus be doubly activated for attack by the bridging hydroxide. Further studies are planned to distinguish between these two mechanistic hypotheses.

ACKNOWLEDGMENT

We thank Ms. Lijin Shu and Mr. Gaofeng Pan for assistance with data collection and help in initial data analysis. We thank Drs. Yang Hai and Mike Sullivan at beamline X9 in NSLS for technical guidance.

REFERENCES

Al-Juaid, S. S., Buttrus, N. H., Eaborn, C., Hitchcock, P. B., Roberts, A. T. L., Smith, J. D., & Sullivan, A. C. (1986) *J. Chem. Soc., Dalton Trans.*, 908−909.

Antanaitis, B. C., Aisen, P., & Lilienthal, H. R. (1983) *J. Biol. Chem. 258*, 3166−3172.

Aquino, M. A. S., Lim, J.-S., & Sykes, A. G. (1994) *J. Chem. Soc., Dalton Trans.*, 429−436.

Armstrong, W. H., & Lippard, S. J. (1984) *J. Am. Chem. Soc. 106*, 4632−4633.

Averill, B. A., Davis, J. C., Burman, S., Zirino, T., Sanders-Loehr, J., Loehr, T. M., Sage, J. T., & Debrunner, P. G. (1987) *J. Am. Chem. Soc. 109*, 3760−3767.

Basha, S. M. M., Bazer, F. W., Geisert, R. D., Roberts, R. M. (1980) *J. Anim. Sci. 50*, 113−123.

Bazzicalupi, C., Bencini, A., Bianchi, A., Fusi, V., Mazzanti, L., Paoletti, P., & Valtancoli, B. (1995) *Inorg. Chem. 34*, 3003−3010.

Beck, J. L., McArthur, M. J., de Jersey, J., & Zerner, B. (1988) *Inorg. Chim. Acta 153*, 39−44.

Borer, L., Thalken, L., Ceccarelli, C., Glick, M., Zhang, J., & Reiff, W. M. (1983) *Inorg. Chem. 22*, 1719−1724.

Bossek, U., Hummel, H., Weyhermüller, T., Bill, E., & Wieghardt, K. (1995) *Angew. Chem., Int. Ed. Engl. 34*, 2642−2645.

Braibanti, A., Pellinghelli, M. A., Tiripicchio, A., Tiripicchio, M., & Camellini, M. (1971) *Acta Crystallogr. B27*, 1240−1244.

Bunker, G., Hasnain, S., & Sayers, D. (1991) In *X-ray Absorption Fine Structure (*Hasnain, S. S., Ed.) pp 751−770, Ellis Horwood, New York.

Chapman, W. H. J., & Breslow, R. (1995) *J. Am. Chem. Soc. 117*, 5462−5469.

Chaudhuri, P., Stockheim, C., Wieghardt, K., Deck, W., Gregorzik, R., Vahrenkamp, H., Nuber, B., & Weiss, J. (1992) *Inorg. Chem. 31*, 1451−1457.

Chen, X.-M., Tong, Y.-X., & Mak, T. C. W. (1994) *Inorg. Chem. 33*, 4586−4588.

Chiari, B., Piovesana, O., Tarantelli, T., & Zanazzi, P. F. (1984) *Inorg. Chem. 23*, 3398−3404.

Clegg, W., Little, I. R., & Straughan, B. P. (1985) *J. Chem. Soc., Chem. Commun.*, 73−74.

Cramer, S. P. (1988) In *X-ray Absorption* (Koningsberger, D. C., & Prins, R., Eds.) pp 257−320, Wiley, New York.

David, S. S., & Que, L., Jr. (1990) *J. Am. Chem. Soc. 112*, 6455−6463.

Davis, J. C., & Averill, B. A. (1982) *Proc. Natl. Acad. Sci. U.S.A. 79*, 4623−4627.

Davis, J. C., Kung, W. S., & Averill, B. A. (1986) *Inorg. Chem. 25*, 394−396.

Dent, P., Lavoinne, A., Nakielny, S., Caudwell, F. B., Watt, P., & Cohen, P. (1990) *Nature 348*, 302−307.

DeWitt, J. G., Bentsen, J. G., Rosenzweig, A. C., Hedman, B., Green, J., Pilkington, S., Papaefthymiou, G. C., Dalton, H., Hodgson, K. O., & Lippard, S. J. (1991) *J. Am. Chem. Soc. 113*, 9219−9235.

Dietrich, M., Münstermann, D., Suerbaum, H., & Witzel, H. (1991) *Eur. J. Biochem. 199*, 105−113.

Doi, K., Antanaitis, B. C., & Aisen, P. (1988) *Struct. Bonding (Berlin) 70*, 1−26.

Dong, Y., Fujii, H., Hendrich, M. P., Leising, R. A., Pan, G., Randall, C. R., Wilkinson, E. C., Zang, Y., Que, L., Jr., Fox, B. G., Kauffmann, K. K., & Münck, E. (1995) *J. Am. Chem. Soc. 117*, 2778−2792.

Drüeke, S., Wieghardt, K., Nuber, B., Weiss, J., Fleischhauer, H.-P., Gehring, S., & Haase, W. (1989) *J. Am. Chem. Soc. 111*, 8622−8631.

Egloff, M.-P., Cohen, P. T. W., Reinemer, P., & Barford, D. (1995) *J. Mol. Biol. 254*, 942−959.

Garrett, T. P. J., Guss, J. M., & Freeman, H. C. (1983) *Acta Crystallogr. C39*, 1027−1031.

Goldberg, J., Huang, H.-B., Kwon, Y.-G., Greengard, P., Nairn, A. C., & Kuriyan, J. (1995) *Nature 376*, 745−753.

Gomez-Romero, P., Casan-Pastor, N., Ben-Hussein, A., & Jameson, G. B. (1988) *J. Am. Chem. Soc. 110*, 1988−1990.

Griffith, J. P., Kim, J. L., Kim, E. E., Sintchak, M. D., Thomson, J. A., Fitzgibbon, M. J., Fleming, M. A., Caron, P. R., Hsiao, K., & Navia, M. A. (1995) *Cell 82*, 507−522.

Hazell, A., Jensen, K. B., McKenzie, C. J., & Toftlund, H. (1994) *Inorg. Chem. 33*, 3127−3134.

Heistand, R. H., II., Roe, A. L., & Que, L., Jr. (1982) *Inorg. Chem. 21*, 676−681.

Jang, H. G., Hendrich, M. P., & Que, L., Jr. (1993) *Inorg. Chem. 32*, 911−918.

Kauzlarich, S. M., Teo, B. K., Zirino, T., Burman, S., Davis, J. C., & Averill, B. A. (1986) *Inorg. Chem. 25*, 2781−2785.
Keough, D. T., Dionysius, D. A., deJersey, J., & Zerner, B. (1980) *Biochem. Biophys. Res. Commun. 94*, 600−605.
Kim, E. E., & Wyckoff, H. W. (1991) *J. Mol. Biol. 218*, 449−464.
Kimura, E. (1994) *Prog. Inorg. Chem. 41*, 443−491.
Kimura, E., Nakamura, I., Koike, T., Shionoya, M., Kodama, Y., Ikeda, T., & Shiro, M. (1994) *J. Am. Chem. Soc. 116*, 4764−4771.
Kirchner, C., & Krebs, B. (1987) *Inorg. Chem. 26*, 3569−3576.
Kissinger, C. K., Parge, H. E., Knighton, D. R., Lewis, C. T., Pelletier, L. A., Tempczyk, A., Kalish, V. J., Tucker, K. D., Showalter, R. E., Moomaw, E. W., Gastinel, L. N., Habuka, N., Chen, X., Maldonado, F., Barker, J. E., Bacquet, R., & Villafranca, J. E. (1995) *Nature 378*, 641−644.
Kistenmacher, T. J. (1972) *Acta Crystallogr. B28*, 1302−1304.
Kitajima, N., Fukui, H., & Moro-oka, Y. (1990) *J. Am. Chem. Soc. 112*, 6402−6403.
Kitajima, N., Tamura, N., Amagai, H., Fukui, H., Moro-oka, Y., Mizutani, Y., Kitagawa, T., Mathur, R., Heerwegh, K., Reed, C. A., Randall, C. R., Que, L., Jr., & Tatsumi, K. (1994) *J. Am. Chem. Soc. 116*, 9071−9085.
Klabunde, T., Sträter, N., Krebs, B., & Witzel, H. (1995) *FEBS Lett. 367*, 56−60.
Klabunde, T., Sträter, N., Fröhlich, R., Witzel, H., & Krebs, B. (1996) *J. Mol. Biol. 259*, 737−748.
Krebs, B., Schepers, K., Bremer, B., Henkel, G., Althaus, E., Muller-Warmuth, W., Griesar, K., & Haase, W. (1994) *Inorg. Chem. 33*, 1907−1914.
Lauffer, R. B., Heistand, R. H., II., & Que, L., Jr. (1983) *Inorg. Chem. 22*, 50−55.
Liu, J., Farmer, J. D. J., Lane, W. S., Friedman, J., Weissman, I., & Schreiber, S. L. (1991) *Cell 66*, 807−815.
McKale, A. G., Veal, B. W., Paulikas, A. P., Chan, S.-K., & Knapp, G. S. (1988) *J. Am. Chem. Soc. 110*, 3763−3768.
Ménage, S., & Que, L., Jr. (1990) *Inorg. Chem. 29*, 4293−4297.
Ménage, S., Zang, Y., Hendrich, M. P., & Que, L., Jr. (1992) *J. Am. Chem. Soc. 114*, 7786−7792.
Miller, S. K., VanDerveer, D. G., & Marzilli, L. G. (1985) *J. Am. Chem. Soc. 107*, 1048−1055.
Minor, W., Steczko, J., Bolin, J. T., Otwinowski, Z., & Axelrod, B. (1993) *Biochemistry 32*, 6320−6323.
Mueller, E. G., Crowder, M. W., Averill, B. A., & Knowles, J. R. (1993) *J. Am. Chem. Soc. 115*, 2974−2975.
Murch, B. P., Bradley, F. C., Boyle, P. D., Papaefthymiou, V., & Que, L., Jr. (1987) *J. Am. Chem. Soc. 109*, 7993−8003.
Murphy, T. B., Johnson, D. K., Rose, N. J., Aruffo, A., & Schomaker, V. (1982) *Inorg. Chim. Acta 66*, L67−68.
Murray, M. K., Malathy, P. V., Bazer, F. W., & Roberts, R. M. (1989) *J. Biol. Chem. 264*, 4143−4150.
Murthy, N. N., & Karlin, K. D. (1993) *J. Chem. Soc., Chem. Commun.* 1236−1238.
Nikolaev, V. P., Khodashova, T. S., Porai-Koshits, M. A., Butman, L. A., & Tsintsadze, G. V. (1985) *Koord. Khim. 11*, 1386−1390.
Nuttleman, P. R., & Roberts, R. M. (1990) *J. Biol. Chem. 265*, 12192−12199.
Ou, C. C., Lalancette, R. A., Potenza, J. A., & Schugar, H. J. (1978)- *J. Am. Chem. Soc. 100*, 2053−2057.
Priggemeyer, S., Eggers-Borkenstein, P., Ahlers, F., Henkel, G., Körner, M., Witzel, H., Nolting, H.-F., Hermes, C., & Krebs, B. (1995) *Inorg. Chem. 34*, 1445−1454.
Pyrz, J. W., Sage, J. T., Debrunner, P. G., & Que, L., Jr. (1986) *J. Biol. Chem. 261*, 11015−11020.
Pyrz, J. W., Pan, X., & Que, L., Jr. (1991) *Inorg. Chem. 30*, 3462−3464.
Quiros, M., Salas, J. M., Sanchez, M. P., Alabart, J. R., & Faure, R. (1991) *Inorg. Chem. 30*, 2916−2921.
Randall, C. R., Shu, L., Chiou, Y.-M., Hagan, K. S., Ito, M., Kitajima, N., Lachicotte, R. J., Zang, Y., Que, L., Jr. (1995) *Inorg. Chem. 34*, 1036−1039.
Riggs-Gelasco, P. J., Stemmler, T. L., & Penner-Hahn, J. E. (1995) *Coord. Chem. Rev. 144*, 245−286.
Roach, P. L., Clifton, I. J., Fülöp, V., Harlos, K., Barton, G. J., Hajdu, J., Andersson, I., Schofield, C. J., & Baldwin, J. E. (1995) *Nature 375*, 700−704.
Roe, A. L., Schneider, D. J., Mayer, R. J., Pyrz, J. W., Widom, J., & Que, L., Jr. (1984) *J. Am. Chem. Soc. 106*, 1676−1681.
Sabirov, V. Kh., Porai-Koshits, M. A., & Struchkov, Yu. T. (1993)- *Koord. Khim. 19*, 81−84.
Scarrow, R. C., Maroney, M. J., Palmer, S. M., Que, L., Jr., Roe, A. L., Salowe, S. P., & Stubbe, J. (1987) *J. Am. Chem . Soc. 109*, 7857−7864.
Scarrow, R. C., Pyrz, J. W., & Que, L., Jr. (1990) *J. Am. Chem. Soc. 112*, 657−665.
Schepers, K., Bremer, B., Krebs, B., Henkel, G., Althaus, E., Mosel, B., & Muller-Warmuth, W. (1990) *Angew. Chem., Int. Ed. Engl. 29*, 531−533.
Schindelmeiser, J., Münstermann, D., & Witzel, H. (1987) *Histochemistry 87*, 13−19.
Scott, R. A. (1985) *Methods Enzymol. 11*, 414−459.
Scott, R. A., & Eidsness, M. K. (1988) *Comments Inorg. Chem. 7*, 235−278.
Spartalian, K., Bonadies, J. A., & Carrano, C. J. (1988) *Inorg. Chim. Acta 152*, 135−138.
Stern, E. A. (1993) *Phys. Rev. B48*, 9825−9827.
Sträter, N., Klabunde, T., Tucker, P., Witzel, H., & Krebs, B. (1995) *Science 268*, 1489−1492.
Suerbaum, H., Körner, M., Witzel, H., Althaus, E., Mosel, B.-D., & Müller-Warmuth, W. (1993) *Eur. J. Biochem. 214*, 313−321.
Taft, K. L., & Lippard, S. J. (1990) *J. Am. Chem. Soc. 112*, 9629−9630.
Teo, B.-K. (1981) In *EXAFS Spectroscopy, Techniques and Applications (*Teo, B.-K., & Joy, D. C., Eds.) pp 13−58, Plenum, New York.
Teo, B.-K., Antonio, M. R., & Averill, B. A. (1983) *J. Am. Chem. Soc. 105*, 3751−3762.
Thich, J. A., Oh, C. C., Powers, D., Vasilou, B., Mastropaolo, D., Potenza, J. A., & Schugar, H. J. (1976) *J. Am. Chem. Soc. 98*, 1425−1433.
Tolman, W. B., Liu, S., Bentsen, J. G., & Lippard, S. J. (1991) *J. Am. Chem. Soc. 113*, 152−164.
True, A. E., Orville, A. M., Pearce, L. L., Lipscomb, J. D., & Que, L., Jr. (1990) *Biochemistry 29*, 10847−10854.
True, A. E., Scarrow, R. C., Randall, C. R., Holz, R. C., & Que, L., Jr. (1993) *J. Am. Chem. Soc. 115*, 4246−4255.
Turowski, P. N., Armstrong, W. H., Liu, S., Brown, S. N., & Lippard, S. J. (1994) *Inorg. Chem. 33*, 636−645.
Vincent, J. B., & Averill, B. A. (1990) *FEBS Lett. 263*, 265−268.
Wahnon, D., Lebuis, A.-E., & Chin, J. (1995) *Angew. Chem., Int. Ed. Engl. 34*, 2412−2414.
Walker, J. D., & Poli, R. (1990) *Inorg. Chem. 29*, 756−761.
Wang, Z., Ming, L.-J., Que, L., Jr., Vincent, J. B., Crowder, M. W., & Averill, B. A. (1992) *Biochemistry 31*, 5263−5268.
Wu, F.-J., Kurtz, D. M., Jr., Hagan, K. S., Nyman, P. P., Debrunner, P. G., & Vankai, V. A. (1990) *Inorg. Chem. 29*, 5174−5183.
Yampolskaya, M. A., Bourosh, I. N., Simonov, Y. A., & Gerbeleu, N. V. (1987) *Zh. Neorg. Khim. 32*, 1655−1659.

BI961436N